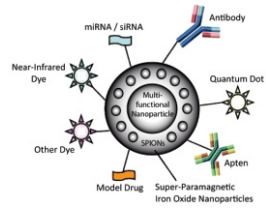
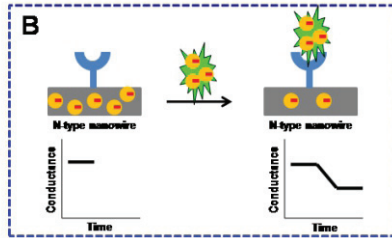
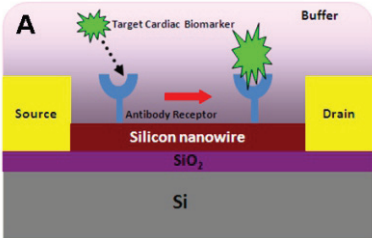
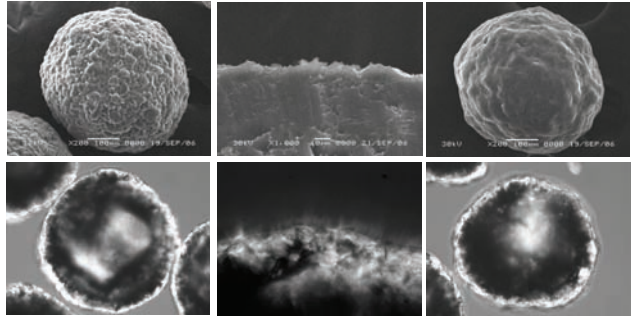
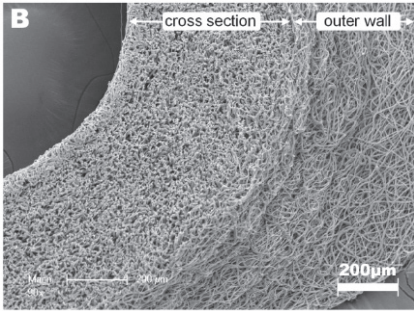


Nanomedicine and the Cardiovascular System



Editors
Ross J. Hunter
Victor R. Preedy

Nanomedicine and the Cardiovascular System

This page intentionally left blank

Nanomedicine and the Cardiovascular System

Editors

Ross J. Hunter

Cardiology Research Fellow
St Bartholomew's Hospital
London
UK

Victor R. Preedy

Professor of Nutritional Biochemistry
School of Biomedical & Health Sciences
King's College London
and
Professor of Clinical Biochemistry
King's College Hospital
UK



CRC Press
Taylor & Francis Group
an informa business
www.crcpress.com

6000 Broken Sound Parkway, NW
Suite 300, Boca Raton, FL 33487
270 Madison Avenue
New York, NY 10016
2 Park Square, Milton Park
Abingdon, Oxon OX14 4RN, UK



Science Publishers
Jersey, British Isles
Enfield, New Hampshire

CRC Press
Taylor & Francis Group
6000 Broken Sound Parkway NW, Suite 300
Boca Raton, FL 33487-2742

© 2012 by Taylor & Francis Group, LLC
CRC Press is an imprint of Taylor & Francis Group, an Informa business

No claim to original U.S. Government works
Version Date: 20111025

International Standard Book Number-13: 978-1-4398-7989-4 (eBook - PDF)

This book contains information obtained from authentic and highly regarded sources. Reasonable efforts have been made to publish reliable data and information, but the author and publisher cannot assume responsibility for the validity of all materials or the consequences of their use. The authors and publishers have attempted to trace the copyright holders of all material reproduced in this publication and apologize to copyright holders if permission to publish in this form has not been obtained. If any copyright material has not been acknowledged please write and let us know so we may rectify in any future reprint.

Except as permitted under U.S. Copyright Law, no part of this book may be reprinted, reproduced, transmitted, or utilized in any form by any electronic, mechanical, or other means, now known or hereafter invented, including photocopying, microfilming, and recording, or in any information storage or retrieval system, without written permission from the publishers.

For permission to photocopy or use material electronically from this work, please access www.copyright.com (<http://www.copyright.com/>) or contact the Copyright Clearance Center, Inc. (CCC), 222 Rosewood Drive, Danvers, MA 01923, 978-750-8400. CCC is a not-for-profit organization that provides licenses and registration for a variety of users. For organizations that have been granted a photocopy license by the CCC, a separate system of payment has been arranged.

Trademark Notice: Product or corporate names may be trademarks or registered trademarks, and are used only for identification and explanation without intent to infringe.

Visit the Taylor & Francis Web site at
<http://www.taylorandfrancis.com>

and the CRC Press Web site at
<http://www.crcpress.com>

Preface

The nanosciences are a rapidly expanding field of research with a wide applicability to all areas of health. They encompass a variety of technologies ranging from particles to networks and nanostructures. For example, nanoparticles have been proposed to be suitable carriers of therapeutic agents whilst nanostructures provide suitable platforms for sub-micro bioengineering. However, understanding the importance of nanoscience and technology is somewhat problematical as a great deal of text can be rather technical in nature with little consideration to the novice. In this series *Nanosciences Applied to Health and Biomedical Sciences* we aim to disseminate the information in a readable way by having unique sections for the novice and expert alike. This enables the reader to transfer their knowledge base from one discipline to another or from one academic level to another. Each chapter has an abstract, “key facts”, applications to other areas of health and disease and a “mini-dictionary” of key terms and phrases within each chapter. Finally, each chapter has a series of summary points. In this book **Nanomedicine and the Cardiovascular System** we cover nanoparticle contrast agents, cell sheet nanotechnology, nanowire field-effect transistors, atomic force microscopy, transfusion medicine, nanoscale topography, nano wire sensor arrays, nanowire transistors, nanospheres, nanomonitor technology, nanospin probes, nanomatrices, vascular grafts, gene transfer using nanomicelles, nanobubbles, biodegradable nanofibers, cholesterol-lowering drugs, thromboses, nanorods, nitric oxide, iron oxide nano particles and stem cells.

Contributors to **Nanomedicine and the Cardiovascular System** are all either international or national experts, leading authorities or are carrying out ground breaking and innovative work on their subject. The book is essential reading for cardiologists, cardiovascular scientists, research scientists, medical doctors, health care professionals, pathologists, biologists, biochemists, chemists and physicists, general practitioners as well as those interested in heart disease and nano sciences in general. **Nanomedicine and the Cardiovascular System** is part of the *Nanoscience Applied to Health and Medicine* series.

The Editors

This page intentionally left blank

Contents

Preface

v

Section 1: General Methods and Applications

- 1. Nanoparticle Contrast Agents for Cardiovascular Medical Imaging** 3
David P. Cormode, Ahmed Klink, Zahi A. Fayad and Willem J.M. Mulder
- 2. Cell Sheet Nano Technology: Engineering and Applications to Cardiology** 25
Yuji Haraguchi, Tatsuya Shimizu, Masayuki Yamato, Ross J. Hunter and Teruo Okano
- 3. Nanowire Field-effect Transistors and Their Applications to Cardiology** 45
Chia-Chang Tsai, Colin R. Martin, Yen-Bin Liu, Chien-Yuan Pan and Yit-Tsong Chen
- 4. Atomic Force Microscopy and the Detection of Nanosized Blood Microparticles** 58
Y. Yuana, M.E. Kuil, T.H. Oosterkamp, R.M. Bertina and S. Osanto
- 5. Nanobiotechnology-based Blood Substitutes and the Cardiovascular Systems in Transfusion Medicine** 77
Thomas Ming Swi Chang
- 6. Collagen Scaffolds and Their Application to Cardiology—the Importance of Matrix Interactions and Nanoscale Topography** 99
Lynn Donlon and Daniel Frankel
- 7. Cardiac Biomarker and Nanowire Sensor Arrays** 121
Guo-Jun Zhang

- 8. Electrical Recording from Cardiac Cells and Tissue Using Nanowire Transistors** 141
Tzahi Cohen-Karni, Bozhi Tian and Charles M. Lieber
- 9. Nanospheres and Applications to Cardiology. Multifunctionality: The Key to Future Success** 164
Andrea Masotti
- 10. Nanomonitor Technology and Its Applicability to Diagnosis of Cardiac Disease** 179
Shalini Prasad, Manish Bothara, Ravikiran K. Reddy, Thomas Barrett and John Carruthers
- 11. Nanospin Probes and Applications to Cardiology** 200
Valery V. Khrantsov and Denis A. Komarov
- 12. Native Endothelium-mimicking Nanomatrices and Applications** 221
Adinarayana Andukuri, Chidinma P. Anakwenze, Bryan A. Blakeney and Ho-Wook Jun
- 13. Nanofibre-based Vascular Grafts** 239
Sarra de Valence, Beat H. Walpoth and Michael Möller

Section 2: Focused Areas, Treatments and Diseases

- 14. Nanoparticle Processing of Cholesterol-Lowering Drug** 263
Toshiro Fukami, Toyofumi Suzuki, Ayyalusamy Ramamoorthy and Kazuo Tomono
- 15. Intratracheal Gene Transfer Using Polyplex Nanomicelles and Their Application to Cardiology** 284
Noriyuki Iwamoto and Mariko Hrada-Shiba
- 16. Use of Microbubbles and Nanobubbles for Diagnostic Vascular Molecular Imaging and Therapeutic Applications** 303
Chih-Hsien Lee, Cheng-An J. Lin, Rajkumar Rajendram and Walter H. Chang
- 17. Multifunctional Nanoagents for the Detection and Treatment of Thromboses** 324
S. Sibel Erdem and Jason R. McCarthy
- 18. Biodegradable Nanofibers in Cardiovascular Medicine: Drug Delivery Application** 345
Masato Mutsuga, Aika Yamawaki-Ogata, Yuji Narita, Makoto Satake, Hiroaki Kaneko and Yuichi Ueda

19. Europium Hydroxide Nanorods and Angiogenic Processes	370
<i>Chitta Ranjan Patra</i>	
20. Iron Oxide Nanoparticles and Cardiac Stem Cells	391
<i>K.W. Au, April M. Chow, Ed X. Wu and H.F. Tse</i>	
21. Nitric Oxide from Nanoparticles and Applications to Cardiovascular Health	407
<i>Pedro Cabrales, Adam J. Friedman and Joel M. Friedman</i>	
<i>Index</i>	427
<i>About the Editors</i>	433
<i>Color Plate Section</i>	435

This page intentionally left blank

Section 1: General Methods and Applications

This page intentionally left blank

Nanoparticle Contrast Agents for Cardiovascular Medical Imaging

David P. Cormode,^{1,a,*} Ahmed Klink,^{1,b} Zahi A. Fayad^{1,c} and Willem J.M. Mulder^{1,d}

ABSTRACT

Over the last ten years, nanoparticles have become increasingly studied as contrast agents for medical imaging. This is due to their unique contrast-generating properties as well as their potentially long circulation half-lives, their high payload and the ease of integrating multiple properties. In particular, they are highly effective for molecular imaging, the non-invasive visualization of the levels of molecules or cell types. Cardiovascular diseases are particularly interesting to study with molecular imaging because of the multiple processes and stages involved and therefore the many cell types and molecules that are important in these diseases. Nanoparticle contrast agents that have been used in conjunction with cardiovascular magnetic resonance

¹Translational and Molecular Imaging Institute, Mount Sinai School of Medicine, One Gustave L. Levy Place, Box 1234, New York, NY 10029.

^aE-mail: davidcormode@gmail.com

^bE-mail: ahmedklink@mac.com

^cE-mail: Zahi.Fayad@mssm.edu

^dE-mail: willem.mulder@mountsinai.org

*Corresponding author

List of abbreviations after the text.

imaging, computed tomography, nuclear imaging techniques or ultrasound include iron oxides, micelles, liposomes, emulsions, gold nanoparticles, quantum dots and lipoproteins. In addition to the above-mentioned technological aspects we highlight several examples of the use of nanoparticles in cardiovascular imaging as case studies at the end of this chapter.

INTRODUCTION

There has been a tremendous focus of research effort on nanotechnology in general and nanoparticles specifically in the past twenty years. Part of the reason for these efforts is that materials confined to nano-sizes (in the range of 1–100 nm in one or more dimensions) can exhibit unusual properties, be it optical, electronic, magnetic, fluorescent or catalytic. A pertinent example of this is quantum dots, semiconductor-based colloids that, when in the size range 1–10 nm, possess extraordinary fluorescent properties. Nanoparticles can be formed from a wide variety of materials, including inorganic materials such as gold, silver, platinum, iron oxide, bismuth and cadmium selenide. Such inorganic materials invariably possess some kind of organic coating, but nanoparticles can also be entirely composed of organic materials such as polymers, amphiphiles, sugars or proteins. Some of these coatings, such as polyethylene glycol, have been found to make nanoparticles highly biocompatible and non-toxic both *in vitro* and *in vivo*. Nanoparticles are now being explored in the biomedical field for drug delivery, gene therapy and medical imaging, among other applications.

Medical imaging is a highly important field, allowing for advanced diagnosis, monitoring of therapy and surgical planning. X-ray imaging is the oldest medical imaging technique, but it is still very widely used. Newer techniques include magnetic resonance imaging (MRI), positron emission tomography (PET) and X-ray computed tomography (CT). These techniques provide three-dimensional datasets of images of patients, as opposed to the two-dimensional images produced by X-ray imaging. Additionally, ultrasound is a widely used technique and fluorescence imaging systems are starting to become available. The details of these different systems are described in a subsequent section. A crucial aspect of all medical imaging systems is image contrast, i.e., visual differences between structures and tissues. There are many ways of generating image contrast, but one way is the use of contrast agents, substances used to enhance the contrast of structures or fluids within the body in medical imaging. This allows, for example, visualization of the vasculature or detection of liver tumors. Contrast agents are either small molecules or

nanoparticles that incorporate some substance that produces contrast for the relevant imaging technique; for example, gadolinium is included in both small molecule contrast agents and nanoparticle formulations to produce contrast in MRI.

In the field of medical imaging, there are several reasons that nanoparticles are attractive for use as contrast agents, as opposed to small molecules. First, nanoparticles may provide unique contrast properties, such as the aforementioned fluorescence of quantum dots or the intense MRI contrast produced by iron oxide nanoparticles. Second, small molecules have a half-life of only a few minutes and the contrast they produce can therefore swiftly dissipate. Nanoparticles, on the other hand, can be designed to have extended half-lives, which can be valuable in cases of image-guided surgery, such as stent emplacement. The extended half-life of nanoparticles would avoid the need to repeatedly inject a small molecule contrast agent. Third, nanoparticles can deliver very high payloads, with as many as *millions* of contrast-generating atoms per nanoparticle as opposed to normally only one such atom for a small molecule. Last, it is relatively straightforward to include multiple components in nanoparticles, such as additional forms of contrast, targeting molecules or therapeutic materials. Inclusion of targeting molecules allows imaging of specific cell types, molecules (e.g., cell surface receptors) or biological processes. This field of targeted imaging is known as molecular imaging. Molecular imaging can allow advanced diagnoses, analysis of therapeutic efficacy and improved information on diseases.

Cardiovascular diseases are the primary cause of mortality in the Western world and consequently their study via imaging is of crucial importance for better understanding of fundamental disease processes, improved diagnoses and the evaluation of (new) therapies. The majority of the work that has been done in nanoparticle-based imaging of cardiovascular disease has focused on molecular imaging. Cardiovascular diseases are also often rather interesting to study, with many different cells and molecules involved and several stages of progression that have distinct levels of expression of cell types and molecular markers. For example, atherosclerosis is a progressive inflammatory disease in which there is a gradual buildup of fatty molecules in the arteries, recruitment of macrophages and other cell types to form tissue deposits known as atherosclerotic plaques (Fig. 1). Eventually, lipid-rich, necrotic or calcified cores develop in these plaques. These plaques sometimes rupture, whereupon a thrombus forms that may occlude the artery and block the blood flow. Ruptures of plaques in the coronary arteries cause 70% of heart attacks. The cell types, molecules and processes of interest include macrophages, endothelial cells, foam cells, smooth muscle cells, vascular cell adhesion molecule 1 (VCAM-1), intercellular adhesion molecule 1,

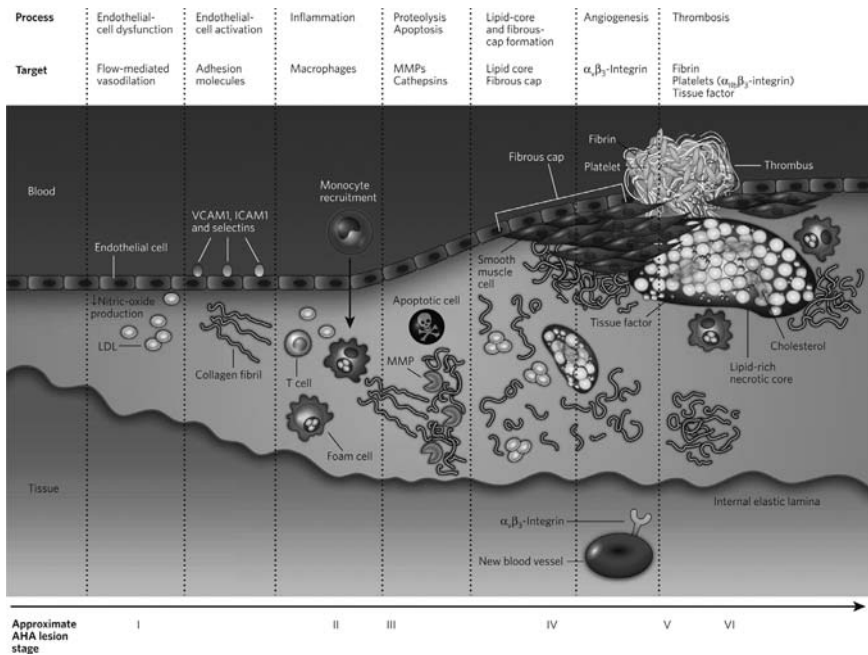


Fig. 1. A simplified depiction of the progression over time of an atherosclerotic lesion, indicating the different processes that occur and receptors expressed at different stages of lesion development. Reproduced with permission from Sanz and Fayad (2008).

Color image of this figure appears in the color plate section at the end of the book.

selectins, collagen, the $\alpha_v\beta_3$ -integrin, matrix metalloproteinases, cathepsins, fibrin, angiogenesis, inflammation, apoptosis and thrombosis (Sanz et al. 2008). Imaging thromboses is discussed in depth in Chapter 17 on multifunctional nanoagents for the detection and treatment of thromboses. From a molecular imaging perspective, it is an interesting challenge to develop contrast agents for these widely differing species, which occur in different locations in the arteries. An additional challenge is the different locations of the vascular beds, i.e., the coronaries in the heart, the aorta and other arteries in the abdomen and the peripheral arteries. An imaging modality-nanoparticle combination that works well in the carotid arteries may not work so well for the coronary arteries, because of the motion of the heart and chest and differences in the surrounding tissue. For these reasons, cardiovascular diseases (e.g., atherosclerosis, myocardial infarction and abdominal aortic aneurysms) have drawn a great deal of interest in the molecular imaging field with many nanoparticles designed to investigate them.

In this chapter we discuss the different types of nanoparticles used as contrast agents in cardiovascular imaging. Subsequently, we discuss how the different imaging techniques work. Last, we give a series of examples of nanoparticles used in cardiovascular disease.

NANOPARTICLES

In this section we describe the different types of nanoparticles that have been used in cardiovascular imaging and highlight some of their most important features.

Nanoparticles can be synthesized from a wide variety of materials and have widely varying structures. Before covering nanoparticle types in depth, first we will discuss a generalized design of nanoparticles for molecular imaging (Fig. 2). These nanoparticles usually have a core and one or more layers of coating materials. The coatings are used to make the nanoparticle hydrophilic and biocompatible. Contrast-generating materials can be located within the core, in the coating or at the coating surface. In the case of gadolinium, for example, contrast is generated with these ions mainly via contact with water, so gadolinium is usually located at the nanoparticle surface, whereas fluorophores do not require contact with water and therefore can be located anywhere within the nanoparticle structure. The availability of different locations in which to load contrast-generating materials or other substances is often exploited to include two or even three types of contrast-generating material in the nanoparticle. In some cases, contrast-generating materials and therapeutics are combined

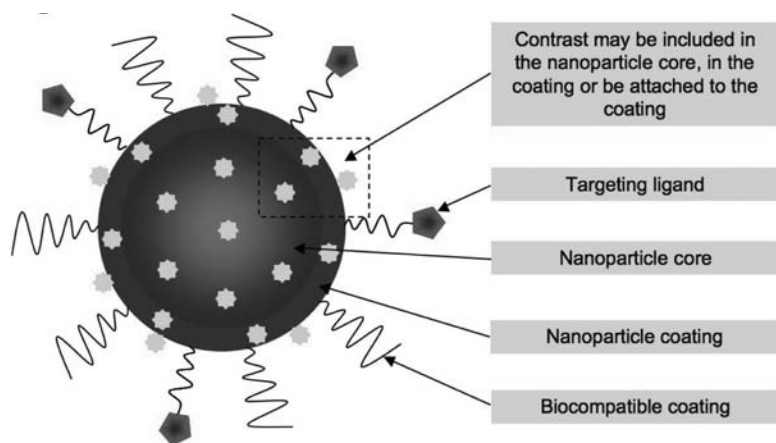


Fig. 2. Schematic depiction of a nanoparticle for use in cardiovascular molecular imaging, indicating the important components. Reproduced with permission from Cormode et al. (2009).

in one nanoparticle to create a “theranostic” formulation. Targeting ligands are normally located at the nanoparticle periphery, to allow the ligand to easily access its target molecule. Placement of the targeting ligand closer to the core could prevent accumulation of the nanoparticle at the desired target site.

The synthesis of nanoparticles can differ greatly, but generally a core or scaffold structure is first created and then subsequently modified. In many cases, the core structure has one or more layers of coating applied, or the coating is modified to make the nanoparticle water soluble and biocompatible. The coating is often designed to include chemical groups, such as amines, carboxylates or maleimides, which can be used to attach metal chelates, fluorophores or targeting ligands to complete the nanoparticle structure.

Iron Oxides

Dextran-coated iron oxide nanoparticles with the trade names Feridex or Sinerem are clinically approved for use as MRI contrast agents in humans. Iron oxide nanocrystals, when placed in a magnetic field, become magnetized and (usually) produce negative contrast in MR imaging because of disruption in the local field experienced by water as the nanoparticles tumble. Sinerem has been used to image macrophages in both animals and humans (see below) via passive targeting. Iron oxides can also be targeted with peptides or antibodies to specific receptors such as VCAM-1, as demonstrated by the group of Weissleder (McCarthy et al. 2007). Iron oxides are almost exclusively used as contrast agents for MRI. Iron oxides have also frequently been used to label cells for cell tracking via MRI, which is discussed in detail in Chapter 20 on iron oxide nanoparticles and cardiac stem cells. While the iron cores used are usually around 5–10 nm in diameter, the overall nanoparticle size can range from 7 to 3500 nm, as some iron oxide agents are embedded in large polymer matrices.

Micelles

Micelles are composed of aggregates of amphiphiles (molecules that have a hydrophobic tail and a hydrophilic headgroup) such as phospholipids (Fig. 3). In a micelle the amphiphiles are arranged such that their hydrophobic tails group together to form the nanoparticle core, while the hydrophilic headgroups face outward towards the aqueous environment. Micelles can be formed from mixtures of different amphiphiles. For example, amphiphiles can be synthesized to possess a metal chelate (containing gadolinium or a radioactive isotope such as copper-64) or a

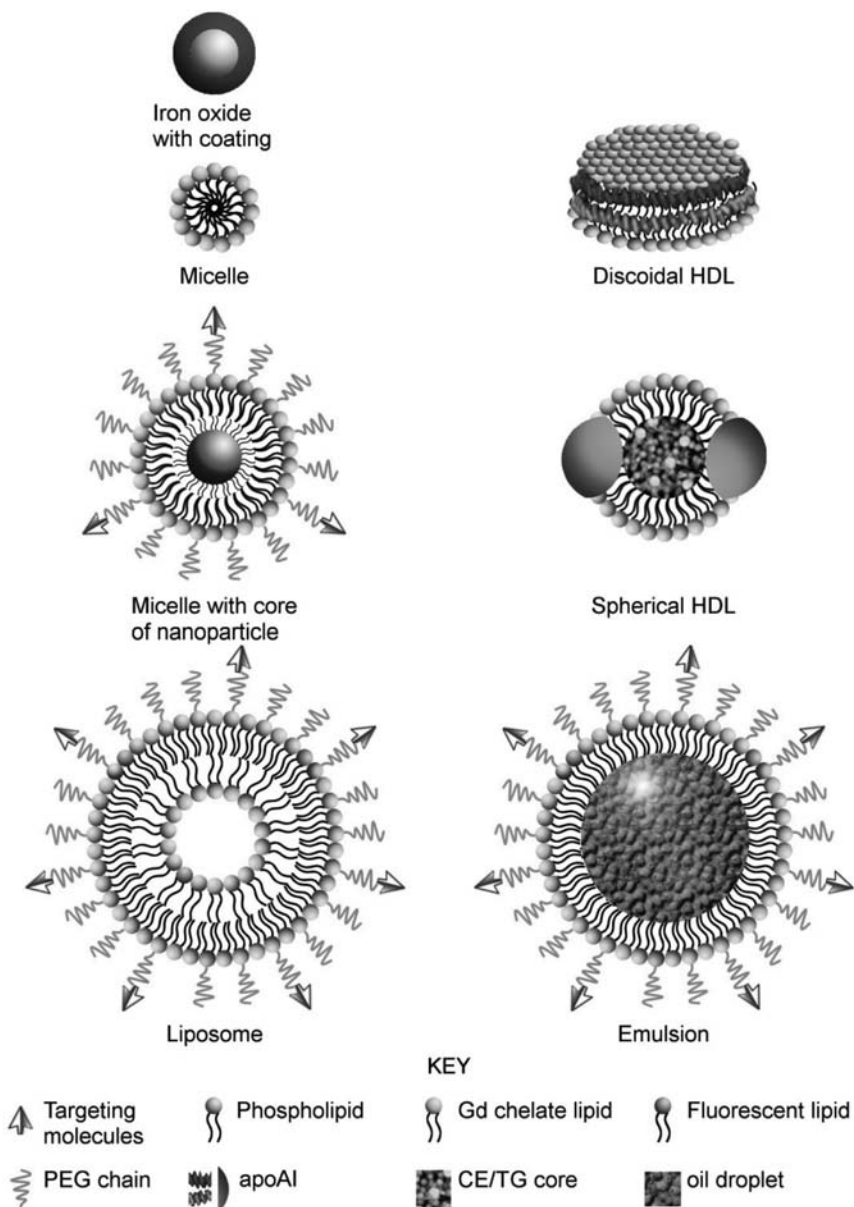


Fig. 3. Schematic depiction of many of the different nanoparticles discussed in this chapter for use in cardiovascular imaging. Reproduced with permission from Chen et al. (2011).

Color image of this figure appears in the color plate section at the end of the book.

fluorophore in their headgroup. These functionalized amphiphiles can be mixed with “carrier” amphiphiles to form the finished micelle. Carrier amphiphiles have no contrast-generating property, but contribute to the structural integrity of the micelle or possess biocompatible features such as polyethylene glycol chains. Additional amphiphiles may be included in the formulation that have functional groups in their headgroup to allow attachment or targeting ligands. Additionally, hydrophobic materials may be included in the micelle core. This may be used to incorporate another type of contrast-generating property in the micelle, because iron oxides, gold nanoparticles or quantum dots can be included in micelle-based contrast agents (Fig. 3). Micelles are generally around 20 nm in diameter, but may be larger if polymeric materials are used. Micelles have been reported as contrast agents for MRI, fluorescence and radioactivity-based imaging techniques.

Liposomes

Similarly to micelles, liposomes are aggregates of amphiphiles, but their structure is quite different, being composed of a lipid bilayer that encapsulates an aqueous core. Liposomes are sized in the 50–500 nm range. This structural change is due to the type of amphiphiles used. To form micelles, amphiphiles with a conical shape are used, with the headgroup larger than the tail. This favors the amphiphiles assembling into a small particle such as a micelle. Amphiphiles that are more cylindrical in shape, such that their headgroup and tail are similar in size, assemble into liposomes, which, being larger, have a lower surface curvature. Contrast-generating materials can be incorporated into liposomes using modified headgroup amphiphiles in the same way as for micelles (Mulder et al. 2009). While hydrophobic materials may be included in the lipid bilayer, this is not often done; it is more common for liposomes to carry hydrophilic contrast-generating materials, such as gadolinium chelates, in their core. Liposomes have been used as contrast agents for virtually every imaging modality.

Oil-in-water Emulsions

Oil-in-water emulsions are composed of oil suspended in water via amphiphiles. The amphiphiles solubilize the nano-sized oil droplets by surrounding the oil with their hydrophobic tails. Contrast-generating materials, therapeutics and targeting ligands can be incorporated in the same way as for micelles, with the additional feature that the oil used to form the emulsion can itself be active as a contrast-generating material. For example, the group of Lanza and Wickline have developed nanoparticle platforms based on perfluorocarbon oils that form emulsions (Lanza et al.

2006). These emulsions can be detected by ^{19}F MR imaging and have been used to investigate many processes in cardiovascular disease, notably angiogenesis and thrombus formation. Moreover, they have been also modified to be detected by ultrasound, CT, ^1H MRI methods, nuclear imaging and optical techniques. Interestingly, drugs have been included in these nanoparticles to make them both therapeutic and diagnostic, or “theranostic”. By tuning the ratio of the oil to the amphiphiles and by altering the amphiphile type, a wide range of nanoparticle diameters can be achieved, i.e., 30 nm to 1 μm .

Gold Nanoparticles

Arguably, gold nanoparticles initiated the tremendous growth of the nanotechnology field seen over the past twenty years, owing to their unique optical, electronic and catalytic properties. They have been extensively studied, so their synthesis is very well developed. For example, their size can be tuned precisely in the 1–100 nm range. As contrast agents, they can be exploited in optical imaging-based techniques, but most reports on gold nanoparticle contrast agents used in cardiovascular applications have focused on CT. Gold nanoparticles are a relatively straightforward method to deliver the large quantities of radio-opaque material needed for CT imaging. There have been several reports on their application as long-circulating vascular phase agents, but more recent studies have been published in which gold nanoparticles have been used to perform targeted imaging of specific cell types. To achieve biocompatibility, their surface can be grafted with many different polymers or proteins. In addition, gadolinium chelates and fluorophores can be attached to the surface to yield additional contrast for MRI and fluorescence techniques.

Quantum Dots

Quantum dots are small (less than 10 nm) semiconductor crystals that have exceptional fluorescence properties (Medintz et al. 2005). They have broadband absorbance and narrow, tunable emission spectra. They do not photobleach like small molecule fluorophores. A significant disadvantage is that they are formulated with high toxicity metals such as cadmium, limiting their potential for use in patients. In addition to yielding fluorescence contrast, several groups have labeled quantum dots with gadolinium chelates for MRI contrast, thus forming bimodal contrast agents. They can be made biocompatible and targeted by the same strategies as the aforementioned agents. Although, as mentioned earlier, quantum dots themselves are small, they can be included in emulsions or other types of nanoparticles, resulting in nanoparticles with an overall diameter that is quite large.

Lipoproteins

There are several lipoproteins: chylomicrons, very low density lipoprotein (VLDL), intermediate density lipoprotein (IDL), low density lipoprotein (LDL) and high density lipoprotein (HDL). They range in size from 10 nm for HDL to over 250 nm for chylomicrons. Lipoproteins are nanoparticles responsible for cholesterol transport in the body, among other functions. They have cores of cholesterol esters and triglycerides, covered in a monolayer of phospholipids. HDL is depicted in Fig. 3. HDL is initially formed without a fatty core, so discoidal HDL (no core) is depicted as well as spherical HDL. Amphiphatic proteins are embedded in the phospholipid coating, which provides structural integrity and targeting.

LDL binds to the LDL receptor, which is overexpressed in cancer, and HDL binds to such receptors as the SR-B1 and ABCA1 receptors, which are overexpressed in macrophages, an important cell type in atherosclerosis. Adapting them as contrast agents allows these important natural nanoparticles to be tracked *in vivo* and provides a method to detect their target receptors (Skajaa et al. 2010). Lipoproteins can be adapted as contrast agents in the same ways as micelles. Lipoprotein contrast agents have been reported for MRI, CT and fluorescence imaging techniques. Despite possessing natural targeting, some formulations have been modified with peptides to be retargeted to other receptors or cell types.

MEDICAL IMAGING TECHNIQUES

Magnetic Resonance Imaging

Magnetic resonance imaging is a primarily non-invasive imaging technique that allows both the morphological and biochemical characterization of tissue. MRI exploits the resonance of atomic nuclei in a massive (0.5–10 T) magnetic field. The most important resonant nuclei for MRI are those of the hydrogen atoms (protons) in water, as water is the most abundant component of the human body. In addition, hydrogen is 100% resonant, while other elements such as carbon contain only a minority of resonant nuclei.

The spin of a proton can be aligned either with or against the magnetic field. In the presence of a very large magnetic field the energy gap between alignment and misalignment is high and a small majority of protons in a sample align their spin with the applied magnetic field. In MRI, first, the protons are excited from the ground state to the higher energy state with pulses of radiowaves at the resonance wavelength of protons. The protons subsequently relax to the ground state and emit radiowaves in the process. These emitted radiowaves are detected and

converted into images. The rate of this relaxation is highly dependent on the environment of the proton and is described by the parameters T_1 and T_2 (longitudinal and transverse relaxation, respectively). Indeed, because of slightly different conditions that exist around the protons in different tissues, an appropriate MR sequence will distinguish tissues depending on their relaxation rate. For example, when using a T_1 weighted sequence, the shorter the T_1 value of a tissue, the faster the protons relax from the excited state to the ground state, the brighter the tissue looks. On the other hand, the shorter the T_2 value of a tissue, the darker the tissue appears on a T_2 weighted sequence.

MRI contrast agents act on the local environment of the protons by decreasing T_1 or T_2 and therefore alter the contrast in their vicinity. Metal ions that are paramagnetic, i.e., have a large number of unpaired electrons, cause protons to relax faster, mostly via coordination interactions. Paramagnetic metals are usually used as T_1 contrast agents. For example, the clinically approved MRI contrast agent Magnevist is composed of Gd^{3+} ions bound to diethylene triamine pentaacetic acid, a chelator. Most agents designed to reduce T_1 contain either Gd^{3+} or Mn^{2+} , which have seven and five unpaired electrons, respectively, and are therefore highly paramagnetic. For molecular imaging with T_1 -based MRI, nanoparticles that include many (100-100,000) paramagnetic metal ions are used, as it is necessary to deliver a large amount of contrast agent to produce a signal change. To reduce T_2 , iron oxide nanoparticles that are superparamagnetic (possessing a magnetic moment only when placed in a large magnetic field) are used, such as the commercially available agents Feridex or Sinerem. These agents produce fluctuations in the magnetic field around them, which causes the affected protons to relax faster. Only nanoparticles can create this effect. It is noteworthy that T_1 and T_2 are inversely proportional to the concentration of contrast agent. Therefore, as reduced T_1 values result in image brightening, T_1 contrast agents such as Magnevist produce brightness in images, whereas Feridex produces dark spots in images, as reduced T_2 values create image darkening.

Computed Tomography

CT was invented in the early 1970s and is the first medical imaging modality made possible by the computer. It is used to produce volumetric images that can be manipulated to reveal various structures in the body based on their density or their ability to attenuate X-rays. CT images are produced by passing X-rays through the body, at a large number of angles via rotation of the X-ray tube around the subject on a single axis (Fig. 5). Multiple linear detector arrays opposite the X-ray source collect the transmitted X-rays and process the data into grayscale images. For

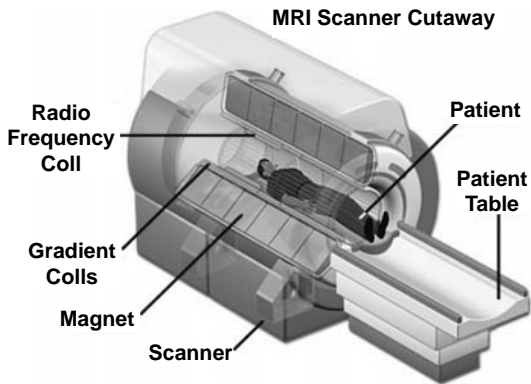


Fig. 4. Schematic of a magnetic resonance imaging system. Reproduced with permission from <http://www.magnet.fsu.edu/>.

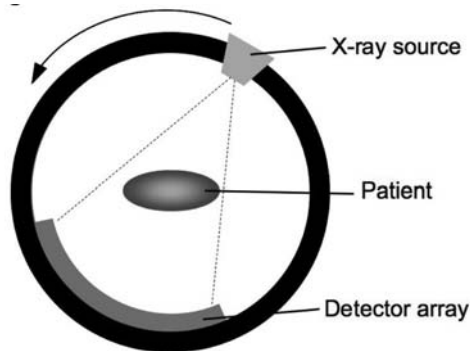


Fig. 5. Schematic diagram of a computed tomography imaging system (unpublished).

example, a dense structure, such as bone, will absorb most of the X-rays and allow only a small proportion of X-rays to pass. The result will be white pixels in the image. On the other hand, air will absorb very little of the X-ray beam, allowing a large number of X-rays to strike the detectors, the result being black pixels in the image.

Clinically approved contrast agents for CT are small molecules that include several iodine atoms and are applied to obtain images of the vasculature. Vascular CT imaging has particular value in cardiovascular disease for identifying atherosclerotic plaques that are occluding the coronary arteries. Iodine is highly X-ray attenuating and therefore results in image brightening in CT images. These agents are rapidly cleared from the circulation. Other elements, such as gold and bismuth, can also be used as a basis for contrast agents. Lately, several groups have reported nanoparticle-based contrast agents for CT (Cai et al. 2007). The advantages of nanoparticles for CT, compared to small molecules, are that they deliver

a very large amount of contrast, they can have long circulation half-lives and they can be efficiently targeted.

Nuclear Imaging

Nuclear medicine describes the branch of radiology in which a chemical or compound containing a radioactive isotope is given to the patient. Rather than yielding information about the anatomy, nuclear imaging images provide information regarding the physiological condition of the patient. For example, cancerous cells have a rapid metabolism and consume a lot of glucose and also a radioactive analog of glucose, ^{18}F -fluorodeoxyglucose. Tumors with an increased glucose uptake will then appear as “hot spots” compared to the rest of the body. The main two nuclear imaging modalities are single photon emission computed tomography (SPECT) and positron emission tomography (PET).

SPECT

In SPECT, a nuclear camera records gamma-ray emissions originating from a radionuclide, from a series of different two-dimensional projections acquired at different angles. A tomographic reconstruction algorithm is then applied to the multiple projections, yielding a three-dimensional data set that can be manipulated to show thin slices along a chosen axis of the body, similarly to other tomographic techniques such as CT or MRI. Typically, a full 360-degree rotation is used to obtain an optimal reconstruction. The total scan time usually varies between 15 and 20 min, although multi-headed gamma cameras can provide accelerated acquisition. Radiotracers used for SPECT emit gamma radiation.

PET

PET is a kind of tomography made possible by the unique fate of positrons. When positrons undergo annihilation by combining with electrons, two 511-keV gamma rays are given off in opposite directions 180 degrees apart. In contrast to SPECT imaging that detects single events, in PET imaging, two detector elements on opposite sides of the subject are used to detect paired annihilation of positrons. PET scans are increasingly integrated alongside CT or MRI scanners (Townsend 2008), the combination giving both anatomic and metabolic information (Fig. 6). Because the two scans can be performed in immediate sequence during the same session, with the patient remaining in the same position, the set of images are precisely co-registered so the areas of PET activity can be correlated with the anatomy obtained on CT or MRI images.

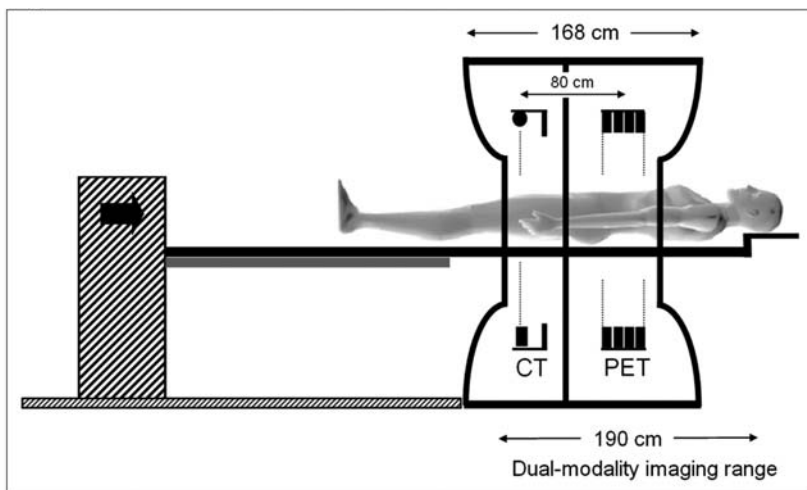


Fig. 6. PET/CT. Sample schematic of the configuration of a dual PET/CT imaging system. Image reproduced with permission from Townsend (2008).

Nanoparticles in Nuclear Imaging

Compared to MRI, CT or ultrasound, nuclear imaging techniques are highly sensitive to contrast agents, as background radiation is very low. Targeted imaging can be fairly easily performed by labeling an antibody or other ligand with a radioactive isotope. Therefore, some of the major motivations for using nanoparticles as contrast agents in MRI, CT or ultrasound, e.g., the delivery of large amounts of contrast or the creation of unique sources of contrast, do not apply in nuclear imaging. Nevertheless, there is some interest in using radiolabeled nanoparticles in nuclear imaging, owing to their favorable pharmacokinetics, the ease of integration of multiple properties in nanoparticles and the ease of validating their targeting with microscopy techniques. Additionally, it is very useful to label nanoparticles with radioactive isotopes in order to facilitate biodistribution studies.

Ultrasound

Ultrasound is a non-invasive diagnostic imaging tool that has improved the diagnosis and management of a number of diseases. Ultrasound has achieved an excellent patient acceptance because it is safe, fast, and inexpensive compared to other imaging modalities. Ultrasound technology produces sectional imaging or slices in multiple planes. An ultrasound machine consists of an ultrasound wave source, a transducer and a computer. The ultrasound transducer emits high-frequency sound

waves, ranging from 1 to 10 MHz. Short bursts of these inaudible high-frequency sound waves are broadcast into the patient by a transducer, and some of the reflected sound waves from body tissues and structures are received by the transducer. The sound waves that are reflected directly back to the transducer are converted into images. Each organ and tissue has its own characteristic echo pattern. Solid organs have a homogeneous echo pattern, whereas fluid-filled organs and masses such as the urinary bladder, cysts and gallbladder have relatively fewer internal echoes. For cardiovascular imaging, ultrasound is frequently performed via use of a catheter inserted into the coronary arteries, a technique known as intravascular ultrasound.

Gas-filled microbubbles are currently the type of contrast agent most often used for ultrasound. These microbubbles oscillate, rapidly contracting and expanding, when they enter a high-frequency ultrasound beam. This phenomenon generates sound waves that can easily be distinguished from the surrounding tissue. Inert gases such as nitrogen or perfluorocarbons are used to form the bubble. In order to protect the gas from diffusing into the bloodstream, the gas core is encapsulated in a shell. Materials such as albumin, lipids or synthetic polymers are used to form this coating. As the name suggests, microbubbles are larger than nanoparticles, but have many of the same design elements and can be specifically targeted.

EXAMPLES OF USE OF NANOPARTICLES IN MEDICAL IMAGING

There are many potential applications of nanotechnology in medicine in general and in medical imaging in particular. For example, iron oxide nanoparticle-based MR contrast agents such as Feridex and Resovist have multiple uses in the clinic. Feridex has a dextran coating, whereas Resovist is a carboxydextran-coated nanoparticle and both are large (60–180 nm) aggregates of coating material that contain multiple iron cores. These agents may be used for liver tumor diagnosis, for example. Sinerem is a smaller iron oxide agent (15–30 nm) and is often referred to as ultrasmall superparamagnetic iron oxides (USPIO). Because of its dextran coating, it has been shown to have an affinity for macrophages. This phenomenon was exploited to image macrophage expression in atherosclerotic plaques induced in rabbits using MRI (Ruehm et al. 2001). The success of such preclinical studies motivated investigators to carry out clinical trials, which proved the feasibility of imaging macrophage infiltration in the carotid atherosclerotic plaques in patients. In the ATHEROMA study, the investigators used the detection of macrophages with Sinerem-enhanced carotid MR imaging to evaluate the anti-inflammatory effect of high dose versus low dose of a lipid-lowering therapy, atorvastatin (Tang et al. 2009).

As shown in Fig. 7, the low dose of atorvastatin applied in patients for 12 wk did not eliminate the accumulation of USPIOs in carotid plaques (the dark spot in the post-USPIO images). However, the authors noticed that USPIO accumulation was eliminated in the plaque starting at 6 wk after the initiation of high-dose treatment, indicating less active macrophages and minimal inflammation in the plaque. At 12 wk, the effect was even more pronounced, as the injection of USPIOs did not provoke any visible MR signal loss in the carotid plaques (Fig. 7G and H). The study was carried out with 20 patients in each group and yielded significant differences in USPIO-defined inflammation, demonstrating the potential of USPIO-enhanced MRI to monitor anti-inflammatory therapies in patients with atherosclerotic lesions.

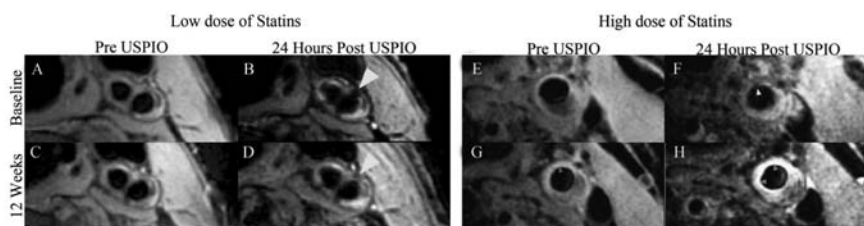


Fig. 7. Molecular imaging in patients. USPIO injection allowed monitoring of the effects of a low dose (left) versus a high dose of statins (right) in patients at 12 wk via MR imaging. A dark spot arising from USPIO uptake in the plaque is still visible after injection of USPIO at 12 wk in the low-dose group (C and D) compared to the baseline (A, B). The high-dose group shows a clear difference in USPIO uptake at 12 wk (G, H). The plaque contains no dark spots, showing the lack of USPIO uptake compared to baseline (E, F). Reproduced with permission from Tang et al. (2009).

Other investigators use iron oxide nanoparticles for cell tracking, as cells can be induced to internalize iron oxide nanoparticles by a variety of methods, which allows the cells to be tracked by MRI as they migrate through tissues. Owing to the high resolution of MRI and the biocompatibility of iron oxide particles, the MRI-iron oxide combination is a popular method for cell tracking, a technique that is of interest to insure proper cell administration and delivery in diseases for which cell therapy is needed, as described in Chapter 20 on iron oxide nanoparticles and cardiac stem cells.

Certain molecules involved in disease formation and progression represent attractive targets for nanoparticle-enhanced imaging, as their detection could lead to early recognition of diseases, better therapeutic management and enhanced understanding of disease progression. In order to develop these site-specific contrast agents, a targeting ligand toward the pathological biomarker of interest is often conjugated to the

nanoparticle. For example, van Tilborg et al. formed paramagnetic and fluorescent micelles from gadolinium chelating lipids, fluorescent lipids, polyethylene glycol (PEG) carrier lipids and maleimide PEG lipids (Fig. 8) that were 22 nm in diameter. Annexin A5 (AnxA5) is a protein specific for phosphatidylserine, which is a phospholipid that is located on the inner side of the cell membrane and is exposed on the outer side of the cell membrane only during apoptosis. AnxA5 was conjugated to the bimodal micelles for the non-invasive assessment of apoptotic cells, which are considered to significantly contribute to atherosclerotic plaque instability. These AnxA5 micelles showed increased MR signal intensity in the aortic vessel wall of atherosclerotic, apolipoprotein knockout (apoE $-/-$) mice 24 h post injection compared to control micelles injected into apoE $-/-$ mice or AnxA5-micelles injected into wild type (WT) mice, as shown in Fig. 8B-G. The presence of AnxA5-targeted micelles in the aorta was confirmed by *ex vivo* near-infrared fluorescence imaging while confocal fluorescence microscopy allowed the precise co-localization of AnxA5-micelles with apoptotic cells and macrophages.

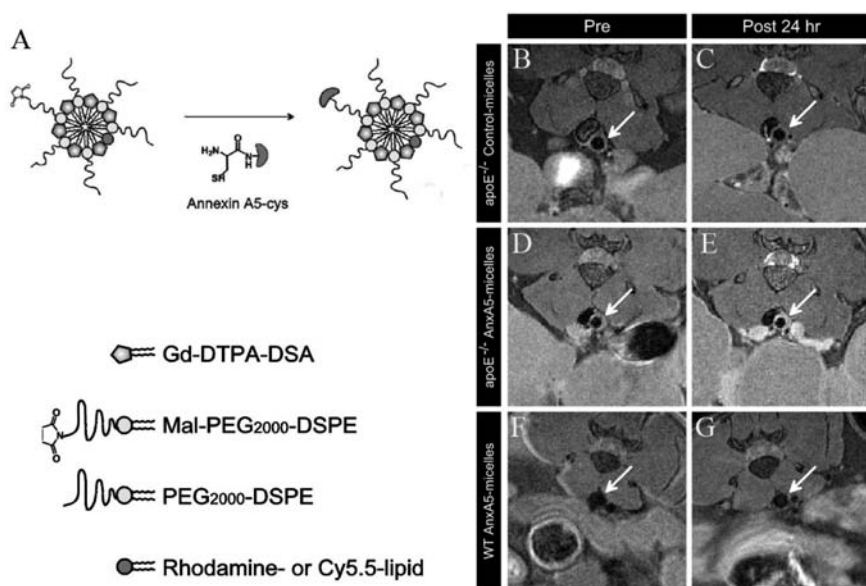


Fig. 8. Detection of apoptosis *in vivo*. (A) Schematic depiction of conjugation of AnxA5 to paramagnetic and fluorescent micelles. (B, C) Typical MR images obtained in atherosclerotic mice before and after injection of control micelles. No enhancement was noticed in that case, whereas injection of AnxA5-micelles produced a bright enhancement in the plaques of atherosclerotic mice (C, D). AnxA5-micelles did not produce any MR signal enhancement in healthy animals (E, F). Reproduced with permission from van Tilborg et al. (2010).

Color image of this figure appears in the color plate section at the end of the book.

Because of its fast imaging capabilities and high resolution, CT also represents an attractive modality for nanoparticle-enhanced imaging in cardiovascular disease. Nanoparticles developed for CT can be used as long-circulating blood pool agents in order to facilitate the visualization of the vasculature over extended periods. Cai et al. developed colloidal gold nanoparticles for imaging the vascular system using CT (Cai et al. 2007). These non-targeted small particles (38 nm) coated with PEG chains proved to be biocompatible and have a half-life of 30 h, which allowed the visualization of the vasculature system from immediately after injection up to 24 h after injection. The authors used these gold nanoparticles to visualize the major vascular structures of mice such as the heart and major arteries as well as smaller vessels using a small animal CT imaging system (Fig. 9A). They also demonstrated the ability of the particles to visualize the small and chaotic vasculature of tumors implanted in mice (Fig. 9B and C). Such nanoparticles could therefore be of great interest to monitor defects of the vascular system and for image-guided surgery.



Fig. 9. Long-circulating CT contrast nanoparticles. Computed tomography angiography obtained with colloidal gold nanoparticles injected in mice (A). Gold nanoparticles allowed the clear visualization of the heart and major vessels as well as small branches. (B) Sagittal view of a tumor neovascularization (arrows) observed after injection of gold nanoparticles. (C) 3D reconstruction of the tumor vascularization allowing the visualization of small and chaotic vessels. Figure reproduced with permission from Cai et al. (2007).

Similarly to MRI, non-invasive visualization of macrophage expression in atherosclerotic rabbits can be performed using computed tomography. Hyafil et al. developed a radiodense nanoparticle contrast agent formed from iodinated cores dispersed in water using a surfactant. This agent was termed N1177 and was used for the detection of macrophages with CT in a rabbit model of atherosclerosis (Hyafil et al. 2007). These plaques typically contain a high level of macrophage infiltration. As can be seen in

Fig. 10, the authors showed that the enhancement of atherosclerotic plaques was significantly higher after the injection of N1177 compared to a small molecule CT contrast agent. The *in vivo* imaging results were corroborated by histological studies that showed a correlation between the density of the lesions assessed by CT after N1177 injection and the macrophage content in the corresponding histological sections. Importantly, the authors confirmed the presence of N1177 nanoparticles inside the macrophage lysosomes using transmission electron microscopy (Fig. 10E and F). Indeed, as shown in Fig. 10G, the electron-dense particles observed in the plaque macrophages exhibited the energy profile of iodine.

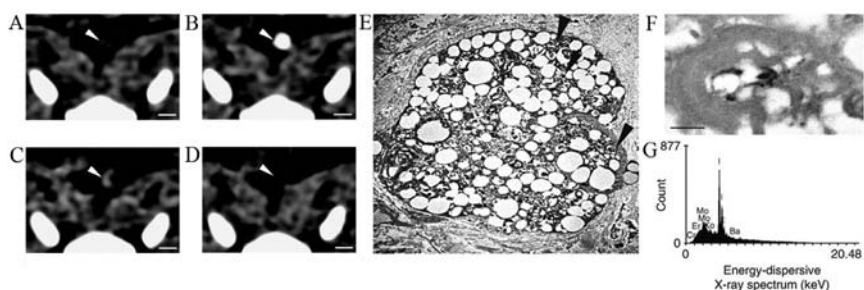


Fig. 10. Macrophage imaging with CT. (A, B, C) Typical images obtained before, during and 2 h after injection of N1177 respectively. Enhancement was observed in plaques 2 h after injection of N1177, whereas no enhancement was observed after injection of a conventional iodine contrast agent (D). (E, F) Transmission electron microscopy showing electron-dense features inside the lysosomes of macrophages 2 h after injection of N1177. (G) The energy profile of these features corresponded to iodine, confirming presence of N1177 in macrophages. Reproduced with permission from Hyafil et al. (2007).

APPLICATIONS TO AREAS OF HEALTH AND DISEASE

Early diagnosis and understanding of disease progression require improvements over conventional imaging techniques. Indeed, anatomical information is very limited and does not permit visualization of the biological processes occurring in the pathophysiology of diseases. Nanoparticles can be engineered to provide superior contrast and therefore facilitate the detection of key pathological information about disease progression. Nanoparticles can be targeted for molecular imaging, allowing the monitoring of disease processes and the effect of various drugs upon these processes, thus providing tremendously valuable information. In addition, nanoparticles can be used for several imaging techniques and can be applied to a wide variety of diseases such as cancer or atherosclerosis.

Key Facts

- Traditional imaging investigates the vasculature and provides anatomical information on the cardiovascular tissues.
- Nanoparticle-enhanced imaging can provide vascular imaging over an extended period or information on biological processes such as apoptosis that are occurring in the cardiovascular tissues. This latter technique is known as molecular imaging.
- Nanoparticles can be formulated to include contrast for MRI, CT, PET, ultrasound and fluorescence as well as therapeutics and targeting ligands, or combinations of these properties.
- Gadolinium or iron oxide is included in nanoparticles to create MRI contrast agents.
- CT nanoparticle contrast agents contain iodine, gold, bismuth or gadolinium.
- Contrast agents for ultrasound are composed of perfluorocarbon or nitrogen gas covered in a polymer, protein or phospholipid shell.
- Nanoparticles can be labeled with isotopes such as copper-64 or fluorine-18 so that they can be detected in PET imaging.
- Quantum dots are inherently fluorescent nanoparticles, but other nanoparticles can be made fluorescent by attaching small molecule fluorophores.

Definitions

Apoptosis: The process of programmed cell death, which occurs in various cardiovascular diseases, weakening tissue.

Computed tomography (CT): An anatomical imaging technique that exploits the varying X-ray absorbance of tissues to create volumetric images.

Macrophages: Inflammatory cells linked to the progression of atherosclerosis and adverse cardiovascular events.

Magnetic resonance imaging (MRI): An anatomical and, to some extent, functional imaging technique that requires a massive magnetic field. Images are formed by transmission to and reception of radiowaves from water protons.

Molecular imaging: “The *in vivo* characterization and measurement of biologic processes at the cellular and molecular level” (Weissleder et al. 2001).

Positron emission tomography (PET): A functional imaging technique that forms images from detection of pairs of gamma rays produced by the annihilation of a positron.

Single photon emission computed tomography (SPECT): A functional imaging technique that detects the emissions of gamma-rays from injected radiopharmaceuticals.

Ultrasound: An anatomical imaging technique that uses very high frequency sound waves.

Summary Points

- Nanoparticles can be formulated that produce image contrast for the majority of medical imaging techniques such as MRI, CT, PET, ultrasound and fluorescence techniques.
- The nanoparticles used in medical imaging can vary in size from 1 to 1000 nm, take a wide variety of morphologies and be composed of many different materials and components.
- Long-circulating nanoparticles can be used to highlight the vasculature for extended periods, as compared with traditional, small molecule contrast agents that are swiftly excreted.
- Nanoparticles can be targeted to specific cells or receptors. When the nanoparticles gather at the targets *in vivo*, imaging can provide an estimate of the level of expression. This is known as molecular imaging.
- Iron oxide nanoparticles are clinically approved and can be used for macrophage imaging in atherosclerosis.
- Preclinically, many processes can be followed in various cardiovascular diseases such as VCAM-1, angiogenesis, macrophages, and apoptosis.

Abbreviations

^1H	:	proton
^{19}F	:	fluorine-19
CT	:	computed tomography
HDL	:	high density lipoprotein
IDL	:	intermediate density lipoprotein
LDL	:	low density lipoprotein
MRI	:	magnetic resonance imaging
PET	:	positron emission tomography
SPECT	:	single photon emission computed tomography
VCAM-1	:	vascular cell adhesion molecule 1
VLDL	:	very low density lipoprotein

References

- Cai, Q.Y., S.H. Kim, K.S. Choi et al. 2007. Colloidal gold nanoparticles as a blood-pool contrast agent for x-ray computed tomography in mice. *Invest. Radiol.* 42: 797–806.
- Chen, W., D.P. Cormode, Z.A. Fayad and W.J.M. Mulder. 2011. Nanoparticles as magnetic resonance imaging contrast agents for vascular and cardiac diseases. *WIREs Nanomed. Nanobiotechnol.* 3, 2: 146–161.
- Cormode, D.P., T. Skajaa, Z.A. Fayad and W.J.M. Mulder. 2009. Nanotechnology in medical imaging: probe design and applications. *Arterioscler. Thromb. Vasc. Biol.* 29: 992–1000.
- Hyafil, F., J.C. Cornily, J.E. Feig et al. 2007. Noninvasive detection of macrophages using a nanoparticulate contrast agent for computed tomography. *Nat. Med.* 13: 636–641.
- Lanza, G.M., P.M. Winter, S.D. Caruthers et al. 2006. Nanomedicine opportunities for cardiovascular disease with perfluorocarbon nanoparticles. *Nanomedicine* 1: 321–329.
- Mccarthy, J.R., K.A. Kelly, E.Y. Sun and R. Weissleder. 2007. Targeted delivery of multifunctional magnetic nanoparticles. *Nanomedicine* 2: 153–167.
- Medintz, I.L., H.T. Uyeda, E.R. Goldman and H. Mattoussi. 2005. Quantum dot bioconjugates for imaging, labelling and sensing. *Nat. Mater.* 4: 435–446.
- Sanz, J., and Z.A. Fayad. 2008. Imaging of atherosclerotic cardiovascular disease. *Nature* 451: 953–957.
- Skajaa, T., D.P. Cormode, E. Falk et al. 2010. High density lipoprotein-based contrast agents for multimodal imaging of atherosclerosis. *Arterioscler. Thromb. Vasc. Biol.* 30: 169–176.
- Tang, T.Y., S.P.S. Howarth, S.R. Miller et al. 2009. The ATHEROMA (atorvastatin therapy: effects on reduction of macrophage activity) study: evaluation using ultrasmall superparamagnetic iron oxide-enhanced magnetic resonance imaging in carotid disease. *J. Am. Coll. Cardiol.* 53: 2039–2050.
- Townsend, D.W. 2008. Dual-modality imaging: combining anatomy and function. *J. Nucl. Med.* 49: 938–955.
- Van Tilborg, G.A.F., E. Vucic, G.J. Strijkers et al. 2010. Annexin A5-functionalized bimodal nanoparticles for MRI and fluorescence imaging of atherosclerotic plaques. *Bioconjugate Chem.* 21, 10: 1794–803.
- Weissleder, R., and U. Mahmood. 2001. Molecular Imaging. *Radiology* 219: 316–333.

Cell Sheet Nanotechnology: Engineering and Applications to Cardiology

Yuji Haraguchi,^{1,b} Tatsuya Shimizu,^{1,c} Masayuki Yamato,^{1,d}
Ross J. Hunter² and Teruo Okano^{1,a,*}

ABSTRACT

Cell-based regenerative medicine has emerged as one of the most promising therapies for patients suffering from severe heart failure and is already being performed in clinical practice. More recently, as an alternative to the direct injection of cell suspensions, advanced therapies have shifted towards the transplantation of tissue-engineered heart grafts. We have developed an original tissue engineering methodology termed “cell sheet engineering” that uses culture surfaces grafted with a temperature-responsive

¹Institute of Advanced Biomedical Engineering and Science, TWIns, Tokyo Women’s Medical University, 8-1 Kawada-cho, Shinjuku-ku, Tokyo, Japan.

^aE-mail: tokano@abmes.twmu.ac.jp

^bE-mail: yharaguchi@abmes.twmu.ac.jp

^cE-mail: tshimizu@abmes.twmu.ac.jp

^dE-mail: myamato@abmes.twmu.ac.jp

²Department of Cardiology, Barts & The London NHS Trust, London, UK.

E-mail: ross.hunter@bartsandthelondon.nhs.uk

*Corresponding author

List of abbreviations after the text.

polymer, poly(*N*-isopropylacrylamide) (PIPAAm), that allows us to control the attachment and detachment of living cells via simple temperature changes. Hence, cultured cells can be harvested as intact cell sheets using the surfaces. Temperature-dependent cell attachment and detachment are controlled by alternating the nanoscale thickness of PIPAAm layers. This unique harvesting method can be performed without proteolytic treatment, preserving extracellular matrix (ECM) on the cell sheets. By layering cell sheets with preserved ECM, various three-dimensional tissues including pulsate myocardial tissues are easily constructed without using the scaffolds that are normally used for holding cells. By using such “intelligent” surfaces, confluent cardiomyocytes can be non-invasively harvested as intact and functional myocardial tissues, without disruption of nanoscale cellular structures, including ion channels and cell-to-cell junctions containing gap junctions. Therefore, electrical coupling within the cardiomyocyte sheet is completely conserved immediately after harvest. Interestingly, after layering, the cardiomyocyte sheets rapidly become electrically synchronized (after approximately 40 min). The preservation of nanoscale cell surface structures (namely gap junction precursors and ECM) are key in the rapid and complete electrical coupling of the layered cardiomyocyte sheets. In addition, electrical interactions between cardiomyocyte sheets can be prevented by inserting non-cardiomyocyte sheets. Conduction delay and conduction block between two cardiomyocyte sheets are observed when multi-layered fibroblast sheets are inserted between them, although this does not occur with a single fibroblast sheet. Polysurgery with cardiomyocyte sheets allows us to create viable and functional heart-like tissue, and transplantation of these multi-layer cardiomyocyte sheets onto the heart leads to functional coupling with native tissue. Transplantation of cell sheets has improved cardiac function in animal models of cardiac injury, with greater therapeutic effects compared to direct injection of cell suspensions. Cell sheet engineering using nanoscale surface chemistry produces cardiomyocyte sheets with preserved cellular surface structures, facilitating integration and electrical coupling with native tissue. There is enormous potential for this technique in treatment of cardiac patients, particularly those with conducting system disease and heart failure.

INTRODUCTION

Cell-based regenerative therapies are currently emerging as some of the most promising methods to treat damaged heart tissue. Regenerative therapy by the direct injection of suspended cells has been clinically performed and shown to produce some limited recovery from heart dysfunction (Menasche et al. 2001). However, with the injection of cell suspensions it is often difficult to control the shape, size, and location that the transplanted cells assume. In addition, significant cell loss due to physical stress, initial hypoxia, or cell wash-out has induced some problems (Zhang et al. 2001). To overcome these problems, myocardial tissue engineering has been viewed as the second generation in cell therapy (Akins 2002). Tissue engineering is currently based on concepts that three-dimensional (3D) scaffolds (for instance, polyglycolic acid, collagen gel, and gelatin) are used as an alternative for extracellular matrix (ECM), and cells are seeded into the scaffolds (Langer and Vacanti 1993). In contrast to these methods that use scaffolds for living cells, our laboratory has developed a unique approach using culture surfaces grafted with a temperature-responsive polymer, poly(*N*-isopropylacrylamide) (PIPAAm), that can control the attachment and detachment of living cultured cells by simple temperature changes. By covalently immobilizing PIPAAm at nanoscale thickness onto conventional culture surfaces, changes in the surface properties can be controlled by simply varying temperature (Yamada et al. 1990; Okano et al. 1993). Above PIPAAm's lower critical solution temperature (LCST) of 32°C, living cells can adhere and proliferate on the surface. The multiplying cells then spontaneously detach themselves when the temperature is reduced below 32°C without any need for enzymatic digestion. Therefore, confluent cultured cells are non-invasively harvested as a contiguous cell sheet, keeping its intact cell-to-cell connections, simply by lowering the culture temperature (Matsuda et al. 2007; Masuda et al. 2008). Additionally, the harvested cell sheet can easily re-attach to other surfaces such as culture dishes, other cell sheets, and host tissues without any "adhesive" (Matsuda et al. 2007; Masuda et al. 2008).

Cardiomyocytes are electrically interconnected with gap junctions (GJs) to allow current to flow from cell to cell, ensuring simultaneous mechanical contraction. Cardiomyocytes cultured on these culture surfaces are also confluent and connect via GJs to synchronize contraction (Oyamada et al. 1994). Therefore, in myocardial tissues prepared by layering cardiomyocyte sheets, it is crucial that electrical and morphological communications are established between the layered cell sheets. In this chapter, we review cell sheet engineering based on nanoscale surface chemistry, the preservation of nanoscale cellular structures in cell sheets, and the characteristics of 3D

myocardial tissues produced using cell sheet engineering. In addition, we describe the application of cell sheet engineering to myocardial tissue in the field of regenerative medicine.

TEMPERATURE-RESPONSIVE CULTURE SURFACE AND CELL SHEET ENGINEERING

Temperature-Responsive Culture Surface

A polymer, PIPAAm, exhibits temperature-responsive hydrophobicity changes in aqueous solutions (Heskins et al. 1968). We have succeeded in the fabrication of PIPAAm-grafted tissue culture polystyrene (TCPS) surfaces using techniques described previously (Yamada et al. 1990; Okano et al. 1993). *N*-isopropylacrylamide (IPAAm) monomer in 2-propanol solution is spread onto TCPS surfaces. These surfaces are then subjected to electron beam irradiation, resulting in the polymerization and covalent grafting of IPAAm to the surface. The nanoscale PIPAAm-grafted layer onto TCPS also shows a temperature-responsive characteristic. At temperatures below 32°C, which is the LCST of PIPAAm molecules, because PIPAAm molecules are highly hydrated, PIPAAm-grafted surfaces become hydrophilic. And at temperatures above 32°C the surfaces abruptly change to hydrophobic because of the extensive dehydration of PIPAAm molecules. This alteration is completely reversible with temperature.

Preparation of Two Different PIPAAm-Graft Surfaces

Cells attach normally to hydrophobic surfaces better than hydrophilic surfaces. Therefore, we have applied the characteristics of PIPAAm-grafted surfaces to cell culture. In fact, cells can attach and proliferate to form a confluent cell monolayer on hydrophobized PIPAAm surfaces at 37°C, above the LCST of PIPAAm molecules, and the confluent cells are detached as a single cell sheet by lowering the culture temperature to 20°C below the LCST (Yamada et al. 1990; Okano et al. 1993; Matsuda et al. 2007; Masuda et al. 2008). The attachment and detachment of cells on PIPAAm-grafted surfaces can be controlled by the hydrophilic/hydrophobic changes of this polymer by simple temperature alterations. The amount of PIPAAm grafted onto TCPS surfaces significantly affects cell attachment (Sakai et al. 1996). A large amount of PIPAAm grafted onto TCPS surfaces inhibits cell adhesion. The detailed mechanism for this remains unclear. Therefore, we analyzed the detailed relationship between the amount of PIPAAm covalently grafted onto TCPS surfaces and the cell attachment/detachment behavior, using two different types of PIPAAm-grafted TCPS surfaces that have different graft amounts. The two different types of

PIPAAm-grafted surfaces were prepared by electron beam treatment after grafting two IPAAm solutions with different concentrations (Akiyama et al. 2004). The amount of polymer on the two PIPAAm-grafted surfaces was determined by attenuated total reflection Fourier transform infrared spectroscopy. The amount of polymer on each surface was $1.4 \pm 0.1 \mu\text{g}/\text{cm}^2$ ($n = 4$, mean \pm SD) and $2.9 \pm 0.1 \mu\text{g}/\text{cm}^2$ ($n = 4$) (Akiyama et al. 2004). Therefore, those two surface types were designated as PIPAAm-1.4 and PIPAAm-2.9, respectively. Though both PIPAAm-grafted surfaces showed hydrophobic/hydrophilic property alterations in response to temperature, PIPAAm-1.4 surface was more hydrophobic than PIPAAm-2.9, both above and below PIPAAm's transition temperature. At 37°C the contact angle (θ) of PIPAAm-1.4 was $77.9 \pm 0.60^\circ$ ($n = 3$, mean \pm SD) and that of PIPAAm-2.9 was $69.5 \pm 1.20^\circ$ ($n = 3$); at 20°C that the contact angle of PIPAAm-1.4 was $65.2 \pm 1.20^\circ$ ($n = 3$) and that of PIPAAm-2.9 was $60.0 \pm 0.06^\circ$ ($n = 3$) (Akiyama et al. 2004). Next, the thicknesses of the grafted PIPAAm layer of PIPAAm-1.4 and PIPAAm-2.9 were measured using a UV excimer laser and an atomic force microscope. First, each PIPAAm-grafted TCPS surface was cleaved by UV excimer laser to expose the TCPS surface. To detect the exposure of hydrophobic TCPS surfaces, the cleaved domains were stained with a hydrophobic fluorescent dye, DiIC18. Next, the thickness of the graft layer was measured by the atomic force microscope. The thickness of the grafted PIPAAm-1.4 or PIPAAm-2.9 was $15.5 \pm 7.2 \text{ nm}$ ($n = 4$, mean \pm SD) and $29.5 \pm 8.4 \text{ nm}$ ($n = 4$) respectively (Akiyama et al. 2004). The thicknesses of two types of PIPAAm-graft surfaces and their hydrophobicities are summarized in Fig. 1.

Control of Cell Attachment and Detachment by Nanoscale Surface Chemistry

Next, cell attachment and detachment behavior on the two PIPAAm-grafted surfaces were examined. Cells attach to the surfaces of PIPAAm-1.4 and proliferate to form a confluent cell monolayer, which is harvested as a single cell sheet by temperature decrease from 37°C to 20°C (Akiyama et al. 2004). Conversely, cells hardly adhered to the surfaces of PIPAAm-2.9 (Akiyama et al. 2004). These results showed that alterations of nanoscale thicknesses of the PIPAAm-grafted layers play a crucial role in temperature-dependent hydrophilic/hydrophobic properties and cell attachment/detachment behavior. Since the cell adhesion protein fibronectin is a major component of ECM and also mediates cell adhesion on culture dish surfaces, the adhesive behavior of fibronectin on PIPAAm-1.4 and PIPAAm-2.9 was also examined. Fibronectin adhered to the surface of PIPAAm-1.4 at 37°C but not at 20°C (Akiyama et al. 2004). However, fibronectin was unable to adhere to the surface of PIPAAm-2.9 at 20°C or

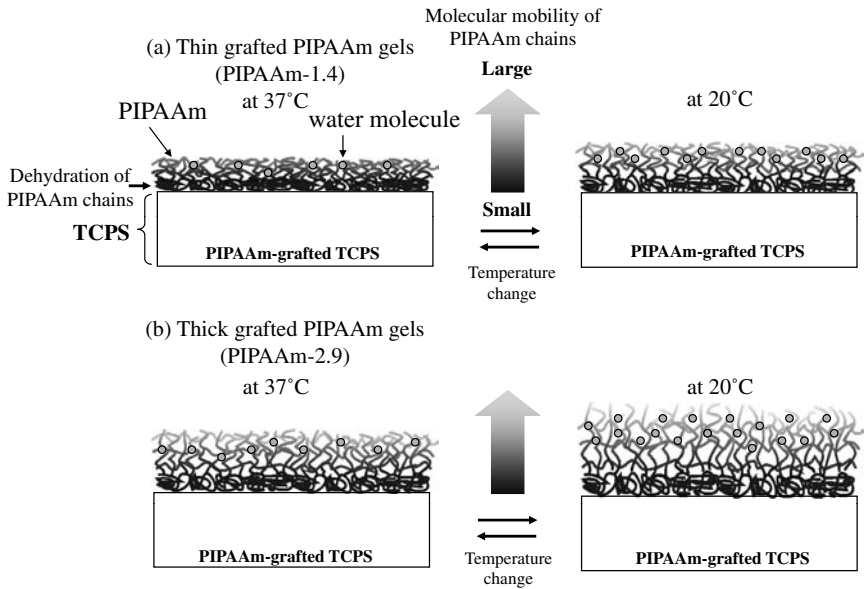


Fig. 1. Schematic diagrams of the influence of molecular mobility of grafted poly(*N*-isopropylacrylamide) (PIPAAm) chains on the hydration of the polymer layers. The grafted PIPAAm layers are thin (a) and thick (b) at 20°C (right side) and 37°C (left side), respectively. The nearer the grafted PIPAAm layers to the interface of tissue culture polystyrene surface (TCPS), the stronger the hydrophobic and restriction of mobility obtained (black layers). Molecular mobility of the grafted polymer layers becomes larger according to the distance from TCPS interfaces (light brown layers). (Reprinted from Akiyama et al. 2004 with permission from American Chemical Society.)

37°C (Akiyama et al. 2004). These behaviors correlate with those of cell attachment, suggesting that cell attachment/detachment behaviors can be controlled by the adherence of cell adhesion proteins. The ability to mobilize the thin cellular layers is strongly influenced by the thicknesses of PIPAAm-grafted layers, since the dehydration of PIPAAm chains is enhanced by the underlying hydrophobic TCPS surface. Cell attachment and detachment are therefore influenced by these subtle differences in thicknesses of the polymer layers. Temperature-dependent cell attachment and detachment are only observed on PIPAAm-grafted surfaces that are approximately 20 nm thick, with no cell adhesion when the grafted layers are thicker than 30 nm. Cell sheets recovered using temperature-responsive “intelligent surfaces” have been applied to tissue engineering and regenerative medicine, and we describe the technology as “cell sheet engineering”.

Preservation of Cell-to-cell Junctions and Extracellular Matrix within Cell Sheets

Cell sheets can be recovered by simple temperature alterations, which induce reversible nanoscale alterations in the thickness of PIPAAm grafted onto TCPS surfaces. Therefore, in the recovery of cell sheets, neither protease nor ethylenediaminetetraacetic acid (EDTA) is required, and consequently cell-to-cell junctions, which are susceptible to damage from protease treatment or the depletion of divalent cations, are preserved intact. Confluently cultured cells can be recovered as intact single cell sheets as shown in Fig. 2A. In addition to cell-to-cell junctions, the presence of fibronectin matrix (which is a major ECM component

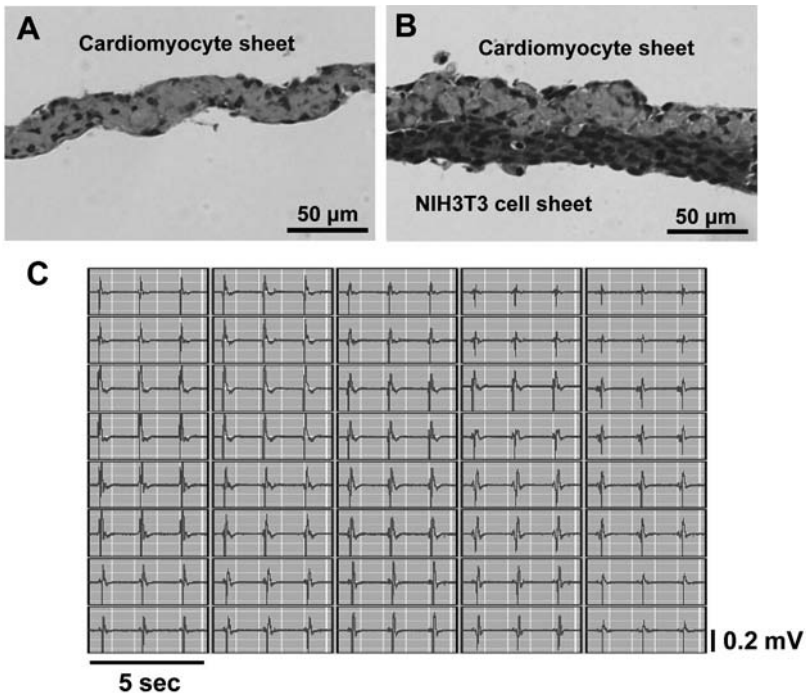


Fig. 2. Cross-sectional views of cell sheets and the electrograms of a cardiomyocyte sheet. A: The cross-sectional view of a single cardiomyocyte sheet. Hematoxylin and eosin staining of the cell sheet shows a cell-dense structure. B: The cross-sectional view of a double-layered cell sheet, a cardiomyocyte sheet (the upper layer) and an NIH3T3 cell sheet (the lower layer). The tight binding of the two cell sheets is detected by hematoxylin and eosin staining. C: Electrical potentials of a single cardiomyocyte sheet just after detachment. Spontaneous electrical potentials are recorded by 40 individual electrodes beneath the cardiomyocyte sheet, and all electrical potentials are completely synchronized. (Unpublished material of the authors.)

Color image of this figure appears in the color plate section at the end of the book.

mediating cell adhesion onto dish surfaces) on cell sheets is detected by immunoblotting and immunohistochemistry (Kushida et al. 1999). The preservation of ECM on the basal surface of cell sheets is also shown by transmission electron microscopy (Kushida et al. 1999). Conversely, after protease treatment fibronectin is only faintly detectable (Kushida et al. 1999). This ECM that is produced during cultivation means cell sheets can be easily attached to other surfaces such as culture dishes, other cell sheets, and even host tissues without any “adhesive” (Matsuda et al. 2007; Masuda et al. 2008). The preserved ECM also means that 3D tissues can be easily created by layering cell sheets without scaffolds (Matsuda et al. 2007; Masuda et al. 2008). For example, in Fig. 2B, a double-layered cell sheet construct, which is fabricated by layering a cardiomyocyte sheet on the top of an NIH3T3 cell sheet, is tightly linked. The construct is very cell-dense since it has been fabricated without scaffolds. The preservation of nanoscale structures such as ECM on cell sheets is therefore important in fabricating 3D tissues without the need for scaffolds or “adhesive”.

APPLICATION OF CELL SHEET ENGINEERING TO MYOCARDIAL TISSUE ENGINEERING

Electrophysiology of a Monolayer Cardiomyocyte Sheet

A sheet of neonatal rat cardiomyocytes detached from a temperature-responsive culture surface was examined histologically and electrophysiologically. The cardiomyocyte sheet is a very cell-dense tissue (Fig. 2A). As the cell sheet shrinks horizontally because of cytoskeletal tensile reorganization, the cardiomyocyte sheet develops several cell layers (Fig. 2A). Because the electrical properties are so important to the functioning of the cardiomyocytes, we examined how these properties are maintained during the recovery process from a temperature-responsive culture surface. The spontaneous action potentials of the cell sheet just after detachment were examined using a multiple-electrode extracellular recording system. The spontaneous action potentials of the cardiomyocytes comprising the sheet were found to be synchronized immediately after recovery (Fig. 2C). This indicates that electrical coupling within the monolayer cardiomyocyte sheet is completely conserved even just after detachment. Therefore, recovery of the cardiomyocyte sheet without the use of any proteases and EDTA allows the cell sheet to preserve its sarcolemmal ion channels and GJs between cardiomyocytes within the cell sheet. Conservation of nanoscale structures on the cell surface and in the extracellular space is important in maintaining tissue functionality. The gentle manner of this unique recovery processes is important as it enables the preservation of this aspect of cell sheets.

Rapid Electrical Coupling of Cardiomyocyte Sheets after Layering

The electrical interaction between two cardiomyocyte sheets after layering was also assessed using the multiple-electrode extracellular recording system (Haraguchi et al. 2006). To detect the action potentials of each cardiomyocyte sheet separately, there was partial overlap of layered cell sheets, with each sheet attached separately to electrodes (Fig. 3A, Haraguchi et al. 2006). Immediately after layering, the two cardiomyocyte sheets activate independently (Fig. 3B). However, after only 34 ± 2 min ($n = 24$, mean \pm SEM), the two layered cardiomyocyte sheets synchronize (Fig. 3C). At this stage, though the excitation cycles of the two cell sheets are synchronized, slight conduction delay is evident. This conduction delay subsequently decreases in a time-dependent fashion (Haraguchi et al. 2006), with complete synchronization and no delay at 46 ± 3 min ($n = 24$) after layering (Fig. 3D). Electrical coupling of a triple-layered

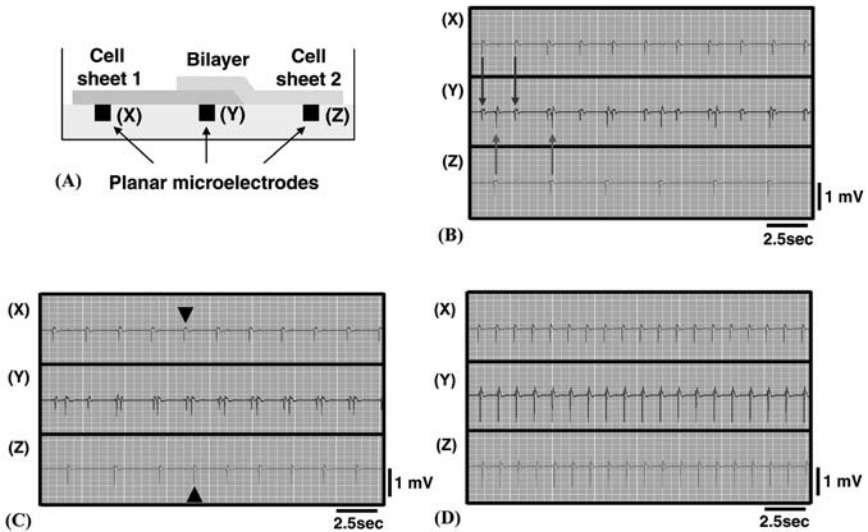


Fig. 3. Rapid synchronization of a layered cardiomyocyte sheet after layering. A: The schematic diagram of a double-layered cardiomyocyte sheet on multi-microelectrodes as viewed from the side. Two cardiomyocyte sheets were layered with partial overlap. Soon after layering, a double-layered cardiomyocyte is independently excited (B). Then, some microelectrodes beneath the monolayer portions detect the spontaneous electrical potentials of individual cell sheet (electrodes X and Z in this figure), while those beneath the overlaid portions detect the electrical potentials of both cell sheets simultaneously (electrode Y in this figure). Arrows indicate the corresponding electrical spikes of each cardiomyocyte sheet. At 34 ± 2 min, two cardiomyocyte sheets begin to couple electrically with slight delays (C). Arrowheads show the start of electrical coupling. At 46 ± 3 min, the excitation spikes of the two cardiomyocyte sheets are coupled completely (D). Data are presented as mean \pm SEM. (Reprinted from Haraguchi et al. 2006 with permission from Elsevier.)

cardiomyocyte sheet is also rapidly established in much the same way at 31 ± 2 min after layering ($n = 3$, mean \pm SD) (Haraguchi et al. 2010). These results show that the electrical coupling of layered cardiomyocyte sheets occurs rapidly and completely. This method of fabricating 3D myocardial tissues without any scaffolds allows rapid and complete electrical coupling of the constituent cells.

Gap Junction Formation in a Layered Cell Sheet

Because GJs are essential for the electrical coupling of cardiomyocytes, it was examined whether GJs form between two cardiomyocyte sheets after a short time period. GJ formation between two cardiomyocyte sheets was detected by fluorescent dye transfer assay (Haraguchi et al. 2006). A membrane-permeable dye, calcein AM, is cleaved within living cells to produce a low-molecular-weight green fluorescent dye, calcein, which is membrane impermeable, but small enough to pass through GJs (Lampe et al. 1994) of diameter approximately 1.5 nm. Calcein transfer from a calcein-loaded cardiomyocyte sheet to a calcein-free sheet was detected at 30 min after layering, and the fluorescence of the unloaded cell sheet increased and expanded time-dependently (Fig. 4A-D). The result suggests that GJ formation occurs within 30 min and increases time-dependently. Because no calcein transfer from the cardiomyocyte sheet to GJ-defective cells is observed (Fig. 4F), calcein should transfer between the layered cell sheets only through GJs, but not via non-specific diffusion of residual calcein AM. Rapid GJ formation is also detected by immunohistological analysis using GJ-related protein, connexin43 (Cx43) antibody (Haraguchi et al. 2006). In addition, Cx43 is detected on non-overlapping cell membrane as well as at cell-to-cell interfaces within a single cardiomyocyte sheet (Haraguchi et al. 2006). Cx43 on the non-overlapping cell membrane is thought to be GJ precursors. GJs are thought to be formed by the docking of two GJ precursors on the cell membranes on adjacent cells. This is dependent on the transcription of Cx43 RNAs, the translation and maturation of Cx43 proteins, vesicular transport, and other factors (Tadvalkar et al. 1983). Therefore, it is thought that electrical coupling between cardiomyocyte sheets is rapid, because cardiomyocyte sheets have GJ precursors already on the cell membranes and GJs at cell-to-cell interfaces. In addition, deposited ECM also promotes the intimate attachment between layered cell sheets and may accelerate the docking of GJ precursors. Preservation of nanoscale cell structures such as GJ precursors and ECM on the cardiomyocyte sheets is therefore important in the rapid and complete electrical coupling of the layered cell sheets. In the case of cardiomyocytes recovered using proteases, no such rapid electrical coupling is observed because both GJ precursors and ECM have been destroyed by these treatments.

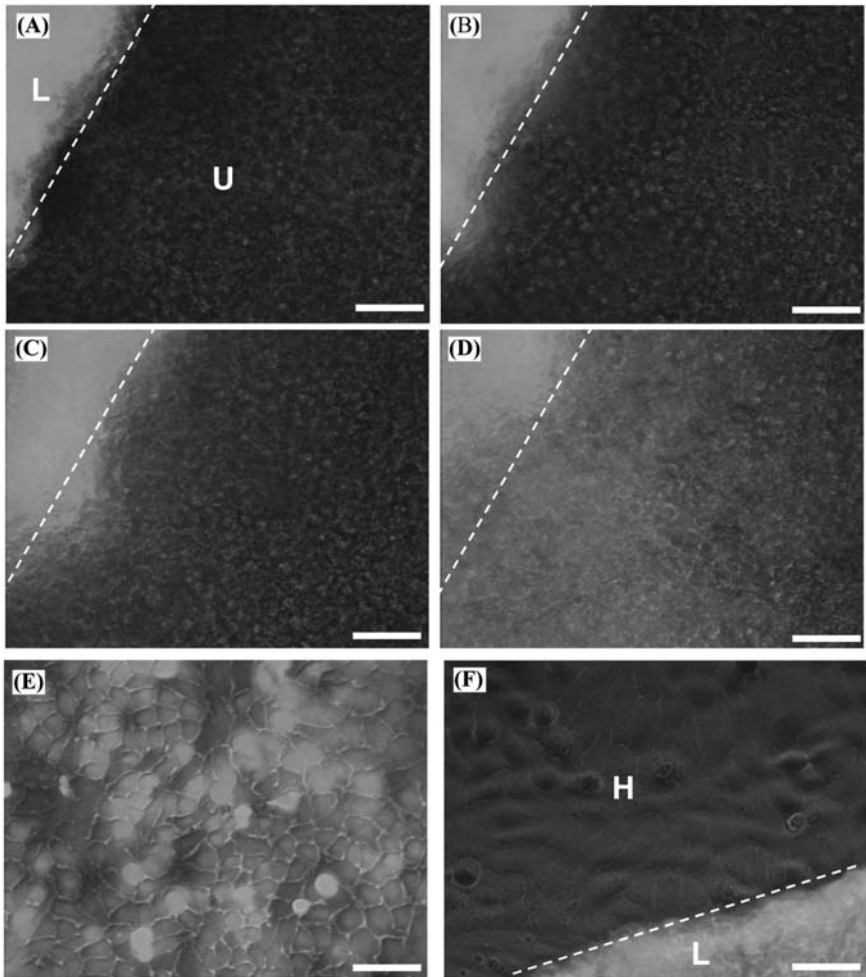


Fig. 4. Fluorescent dye transfer between a double-layered cardiomyocyte sheet. A calcein AM-loaded cardiomyocyte sheet was layered on top of an unloaded cardiomyocyte sheet. Fluorescent pictures at the border region of the layered cardiomyocyte sheet were taken at 0 min (A), 30 min (B), 60 min (C), and 120 min (D) after layering. Calcein transfer to the unloaded sheet is observed at 30 min and expanded time-dependently. Though HeLa cells, which are GJ-negative cells, have the ability to take in calcein AM directly (E), no dye transfer from a calcein-loaded cardiomyocyte sheet (L) to the confluent HeLa cells (H) is observed even after 120 min (F). Broken lines show the border regions between the calcein-loaded cardiomyocyte sheet and unloaded cardiomyocytes or HeLa cells. L: calcein AM-loaded cardiomyocyte sheet; U: unloaded cardiomyocyte sheet; H: confluent HeLa cells. Scale bars show 50 μm . (Reprinted from Haraguchi et al. 2006 with permission from Elsevier.)

Color image of this figure appears in the color plate section at the end of the book.

Time Course of Electrical Coupling of a Layered Cardiomyocyte Sheet

The mechanism we have proposed for the electrical coupling of two cardiomyocyte sheets after layering is illustrated in Fig. 5. At first, the action potentials of two cardiomyocyte sheets are dissociated (Fig. 3B). This shows that no electrical coupling is yet established between two cardiomyocyte sheets, because there are too few GJs connecting them. The electrical excitations arising from the pacemaker cells of each cardiomyocyte sheet are conducted independently throughout the intact cell sheets. Therefore, two independent action potentials are detected at electrodes beneath the layered portion (Figs. 3B and 5A). The cardiomyocyte sheets synchronize electrically with slight delays at 34 ± 2 min after layering (Fig. 3C). After adequate GJs are formed between the two cardiomyocyte sheets, electrical excitation from the more rapidly depolarizing cell sheet, namely the pacemaker cell sheet (cell sheet 1 in Fig. 5B), is conducted to

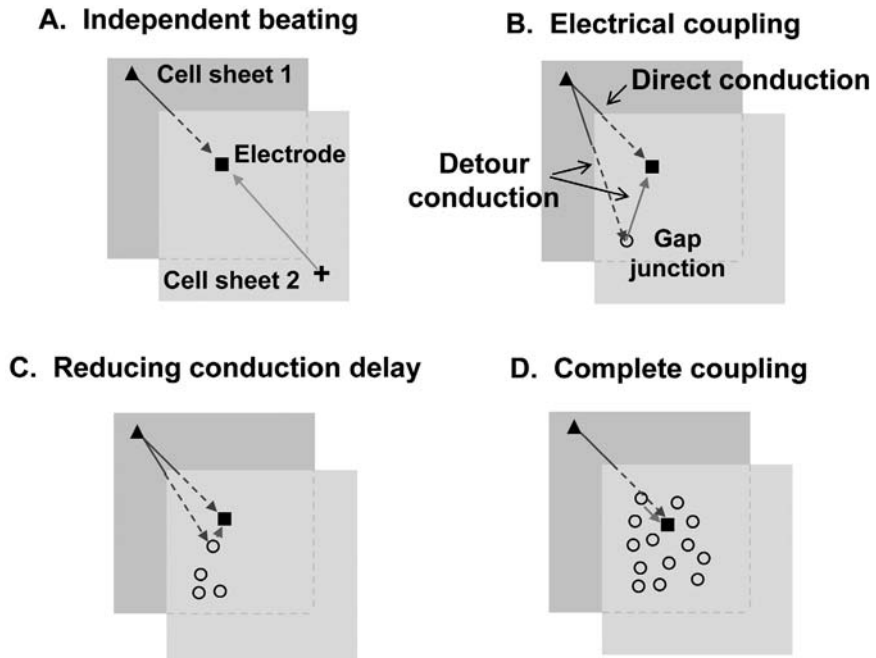


Fig. 5. Electrical conduction routes of coupled cardiomyocyte sheet layers. A: Before electrical coupling between two cardiomyocyte sheets. B: After electrical coupling with slight conduction delay. C: The conduction delays diminish in time-dependent manner due to random GJ formation. D: Complete coupling between two cardiomyocyte sheets. Arrows show electrical conduction in cardiomyocyte sheets. Squares and circles show electrodes and GJs, respectively. (This figure is our hypothesis and is unpublished.)

and propagates through the other cell sheet, namely the non-pacemaker cell sheet (cell sheet 2 in Fig. 5B). At this point, electrical signals reach electrodes through the two independent routes, both directly through the pacemaker cell sheet and indirectly through the non-pacemaker cell sheet having conducted through a small number of GJs (Fig. 5B). It is thought that these two conduction routes are the source of the observed delays. These delays decrease in a time-dependent fashion (Haraguchi et al. 2006), suggesting that (1) additional GJs are randomly formed at the overlapped part of the layered cell sheets and (2) the electrical impulse is conducted to the non-pacemaker cell sheet through the fastest possible route (Fig. 5C). At 46 ± 3 min after layering, the impulses propagate across both cell sheets to separate electrodes simultaneously, suggesting complete coupling has been established, by the formation of GJs throughout the interface between the layered cell sheets (Figs. 3D and 5D). During this process, GJs are formed by the docking of nanoscale GJ precursors on the surface of adjacent cell sheets. Greater understanding of basic tissue-to-tissue communications of myocardial tissues has allowed insight into this process.

Electrical Interaction of Separated Cardiomyocyte Sheets

In addition to electrical interactions between neighboring cardiomyocytes, interactions between separated cardiomyocytes are also important in the understanding of normal heart function and pathological states. Therefore, we analyzed the electrical interactions between separated cardiomyocytes prepared by cell sheet engineering (Haraguchi et al. 2010). Complete electrical coupling of two separated cardiomyocyte sheets occurs when an NIH3T3 mouse fibroblast sheet is inserted between them (Fig. 6A, Haraguchi et al. 2010). However, when a double-layered NIH3T3 cell sheet is inserted between two cardiomyocyte sheets, although they synchronize, the electrical coupling between them is incomplete and conduction delays are observed (Fig. 6B, Haraguchi et al. 2010). When a triple-layered NIH3T3 cell sheet is inserted, the electrical coupling of two cardiomyocyte sheets is completely blocked (Fig. 6C, Haraguchi et al. 2010). The physical distance between the two separated cardiomyocyte sheets prevents formation of GJs and results in failure of electrical coupling, and consequently conduction delay or block. Analyses of impulse propagation, conduction delay and block in cell sheets may provide an experimental model for the study of cardiac arrhythmia. The opportunity to examine the effect of antiarrhythmic drugs may help to elucidate their therapeutic mechanisms and aid further drug development.

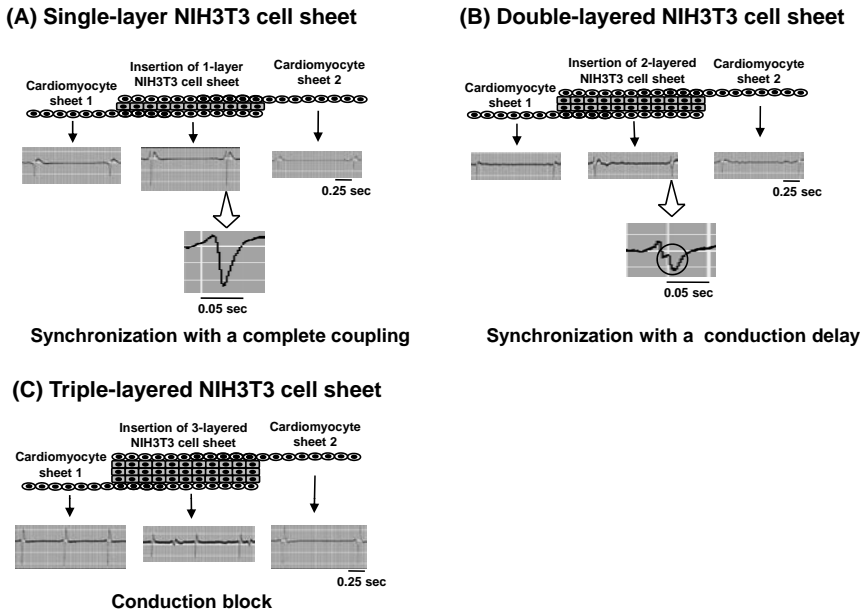


Fig. 6. Conduction delay and block between separated cardiomyocyte sheets caused by insertion of a layered NIH3T3 mouse fibroblast sheet. A single NIH3T3 cell sheet (A), a double-layered NIH3T3 cell sheet (B), or a triple-layered NIH3T3 cell sheet (C) was inserted between two cardiomyocyte sheets. Electrical potentials were monitored by a multiple-electrode extracellular recording system. In the case of single NIH3T3 cell sheet insertion, two cardiomyocyte sheets are completely coupled at 154 ± 41 min after layering (A) ($n = 5$, mean \pm SD, Haraguchi et al. 2010). On the other hand, in the case of double-layered NIH3T3 cell sheets insertion, two cardiomyocyte sheets do not completely couple, though those cell sheets are synchronized (B) (Haraguchi et al. 2010). Two cardiomyocyte sheets are unable to synchronize when a triple-layered NIH3T3 cell sheet is inserted between them (C) (Haraguchi et al. 2010). A circle in (B) shows a conduction delay. (This figure is unpublished.)

3D MYOCARDIAL TISSUE RECONSTRUCTION *IN VIVO* AND THERAPEUTIC EFFECTS BY CELL SHEET TRANSPLANTATION

When layered cardiomyocyte sheets are transplanted into the dorsal subcutaneous tissues of nude rats (see Definitions), the beating of the transplanted grafts can be observed macroscopically and continue for up to 1 year (Shimizu et al. 2003). Interestingly, electrograms derived from transplanted grafts are detected independently from the host heart (Shimizu et al. 2003). In addition, repeated transplantations 24 h apart (or polysurgery) of triple-layer cardiomyocyte sheets produces a thick (approximately 1 mm) cell-dense myocardium with a well-organized microvascular network (Shimizu et al. 2006). The spontaneous and